The effect of a finite interaction region on the measurement of coherence parameters in electron-photon coincidence experiments

J. Phys. B: At. Mol. Opt. Phys. **24** (1991) 1049–1067. Printed in the UK

The effect of a finite interaction region on the measurement of coherence parameters in electron–photon coincidence experiments

P J M van der Burgt, J J Corr and J W McConkey

Department of Physics, University of Windsor, Ontario N9B 3P4, Canada

Received 11 May 1990, in final form 7 November 1990

Abstract. Electron–photon coincidence experiments are usually carried out by crossing an electron beam with a beam of atoms emerging from a capillary tube or array. Recently it has been found that the finite dimensions of the interaction region formed by the crossing beams can affect the coherence parameters that are measured in these experiments. We have developed models with which these effects and those related to the finite acceptance angles of the detectors can be simulated numerically. This article presents a description of the models and presents results which illustrate the possible magnitude of these effects in electron–rare gas scattering experiments. Other depolarizing effects such as internal atomic interactions are also discussed.

1. Introduction

The most detailed information about the formation of atomic excited states in electron collisions with atoms is obtained in coincidence experiments, in which scattered electrons and emitted photons are detected in coincidence. The large amount of experimental and theoretical data obtained in this field has been reviewed extensively most recently by Andersen *et al* (1988) and Slevin and Chwirot (1990). These studies are concerned with not only the determination of excitation amplitudes for the production of particular eigenstates but also with information about the coherence between excitation amplitudes.

In these experiments collisions between electrons and atoms are taking place in a small interaction region formed by the intersection of an electron beam of well defined energy and diameter, and a jet of atoms flowing out of a narrow tube or array of tubes into the vacuum. Although the dimensions of the interaction region are finite, they are usually much smaller than the distances from the interaction region to the photon detector and to the entrance aperture of the electron energy analyser. It is therefore often tacitly assumed that the finite dimensions of the interaction region do not affect the signals obtained by the photon detector and the electron energy analyser.

Recently Zetner *et al* (1989, 1990) obtained strong indications that, under certain circumstances, effects due to a finite size of the interaction region play a significant role. Repeating an earlier experiment by Register *et al* (1983), they studied the superelastic scattering of electrons from laser-excited $^{138}Ba\ ^1P_1$ atoms. Despite extensive testing of the experimental conditions, they were not able to eliminate unexpected asymmetries in the observed signals. They performed a detailed study and model calculation of the effects of a finite interaction region. Their calculations show that

0953-4075/91/051049+19$03.50

the finite interaction region can severely affect the observed superelastic scattering intensity, even at scattering angles significantly different from zero degrees.

Because electron–photon coincidence experiments can be viewed as the time inverse of superelastic scattering experiments, it is to be expected that similar effects play a role in these experiments as well. Indeed a number of recent measurements obtained in this and other laboratories (Danjo *et al* 1985, Nishimura *et al* 1986, Plessis *et al* 1988, Murray *et al* 1989) show disagreements between measured and calculated Stokes parameters. The disagreements occur most obviously in the linear polarization of the radiation emitted in the scattering plane perpendicular to the electron beam (P_4 parameter). Because information concerning spin-dependent processes is deduced from these parameters, assessment of possible effects due to a finite interaction region is of extreme importance and has recently been emphasized (Martus *et al* 1988, Martus and Becker 1989, Hanne 1990, McConkey *et al* 1990). Very recently Simon *et al* (1990) have carried out a careful study of small angle scattering from Hg using electron-polarized photon coincidence techniques and have highlighted the care which must be taken to properly allow for these effects.

In this paper we present a detailed investigation of the effects of a finite interaction region on the measurement of coherence parameters in electron–photon coincidence experiments. The motivation for the present work stems from the importance of a comparison between theory and experiment, and the realization that the issue is not resolved by staying away from measurements at scattering angles less than 15° or by merely increasing the error bars on the experimental data points. The present work entails model calculations based on theoretically calculated coherence parameters, a comparison with experimentally obtained results, and an assessment of the extent that the effect can be minimized by control and adjustment of the essential experimental parameters.

In a companion paper (Corr *et al* 1991) we discuss a wide range of Stokes parameter measurements using heavy rare gas targets. The results of this paper are used in the analysis of that data.

In section 2, we give a description of our experimental set-up, in section 3 we present a detailed discussion of our method to model various effects related to the finite size of the interaction region, in section 4 we give examples illustrating the magnitude of the effects which can occur and in section 5 we discuss the effects of internal atomic interactions. Our findings are summarized in section 6.

2. Experimental apparatus

The experimental apparatus has been discussed in earlier papers (see Plessis *et al* (1988) for a schematic of the apparatus), and so we give only a brief description here. Some additional pertinent details are given in the following paper in which we discuss in detail our measurements on coherence in heavy rare gas excitation.

An electron beam produced by a simple electron gun is crossed with a gas jet, and electrons scattered from the interaction region formed by the intersection of the beam and the gas jet with well defined energy and scattering angle pass through an electrostatic energy analyser and are detected by a channeltron. The plane formed by the direction of the incident and the scattered electrons is the nominal scattering plane. Theoretical analysis (see next section) shows that at most five real parameters pertaining to the excited state can be determined. The relevant parameters in our experiment are (i) the

three Stokes parameters of the radiation emitted perpendicular to the collision plane (P_1, P_2 and P_3 parameters), and (ii) the linear polarization of the radiation emitted in the scattering plane perpendicular to the electron beam (P_4 parameter). The fifth parameter, the total intensity of the emitted radiation, is not measured in our experiment. Our experiment focuses on the excitation of $ns'[\frac{1}{2}]_1^0$ and $ns[\frac{3}{2}]_1^0$ states of the heavy noble-gas atoms. These levels radiate in the VUV so that polarization analysis has to be performed utilizing the reflection properties of gold-coated reflectors (see Westerveld *et al* 1985).

In order to study the effects of a finite interaction region more effectively, we modified the gas inlet system shown in figure 1 of Plessis *et al* (1988) by adding a second gas jet perpendicular to the scattering plane. In practice we found that data taken using the two systems were identical.

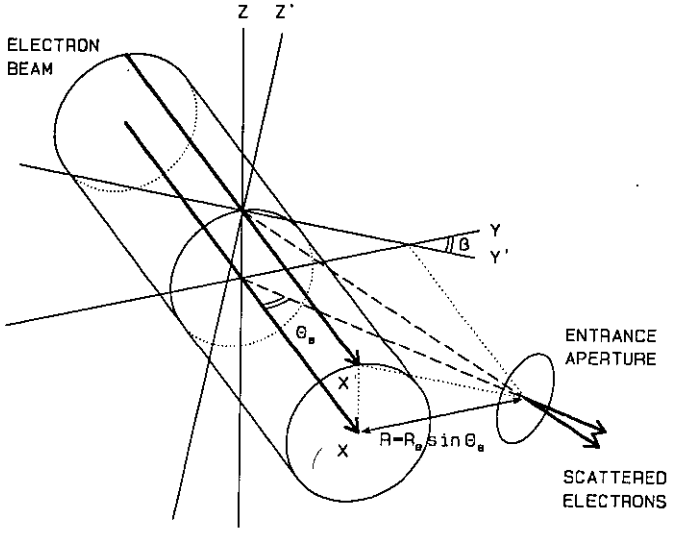

Figure 1. Schematic diagram illustrating the scattering situations discussed in the text in connection with the analytical model (section 3.4). Electrons scattered into the electron energy analyser from the centre or top of the electron beam define the x, y and x', y' scattering planes respectively. The planes are rotated from one another through an angle β.

3. Theoretical Models

3.1. Introduction

As a starting point for a detailed discussion of the effects of a finite interaction region consider a scattering event occurring at a point displaced vertically from the nominal scattering plane at the top of the electron beam. This is illustrated in figure 1. In this case the scattered electron passes from the top of the electron beam through the entrance aperture, so that for this particular event a scattering plane is defined by the x' and y' axes, as shown in figure 1. In this geometry the x-axis is chosen coincident with the centre of the electron beam, and the y-axis is chosen such that the entrance aperture is in the x–y plane, which is the nominal scattering plane. This choice of

coordinate frame is commonly called the natural frame, and will be used throughout this paper.

For the event described above the scattering plane is rotated with respect to the nominal scattering plane and the scattering angle is slightly different from the nominal scattering angle. For both reasons the intensity and the polarization will be somewhat different from the intensity and the polarization from the centre of the interaction region, and a possible spurious effect on the measured signals will occur. In our model calculations we will also look at the effect of a small displacement of the electron beam caused, for example, by mechanical misalignment of the system or by electrostatic deflection. For this purpose we consider the nominal scattering plane to be defined by the axis of the electrostatic lens elements of the electron gun (x-axis) and the position of the centre of the entrance aperture of the electron energy analyser. The centre of the interaction region is defined as the point where the rotation axis of the analyser crosses the electron gun axis.

In general possible effects due to the finite collision region may exist, related to the finite size and displacement of the electron beam, the finite size of the gas jet, the preferential acceptance of scattered electrons away from the nominal scattering centre due to misfocusing of the energy analyser, and the variation of the intensity and polarization of the emitted radiation as a function of scattering angle. In addition possible effects could occur due to the acceptance angle of the photon detectors, and the acceptance angle of the electron energy analyser (diameter of the entrance aperture). In the following sections we shall discuss how all these effects can be incorporated into a numerical model, enabling us to study the effects of a finite interaction region.

3.2. Intensity and polarization of the emitted radiation

In a typical electron–photon coincidence experiment the coincidence rate per unit scattering volume, involving coincident scattering of an electron in a solid-angle element $d\Omega_e$ and emission of a photon of polarization $\hat{\varepsilon}$ in $d\Omega_p$, can be written as (Macek and Jaecks 1971):

$$N(\hat{\varepsilon}) = \frac{\omega^3}{2\pi\hbar c^3} d\Omega_e \, d\Omega_p \, \mathrm{Tr}_f \, \hat{\varepsilon}^* \cdot \mu_{if} \rho_i \mu_{if} \cdot \hat{\varepsilon}. \tag{3.1}$$

Here ω is the frequency of the emitted photons, μ_{if} is the electric dipole operator between the initial excited state $|i\rangle$ and the final state $|f\rangle$ of the atom, and ρ_i is the density matrix of the excited atoms decaying within the resolution time of the coincidence apparatus. Following Nienhuis (1980) we introduce the 3×3 Cartesian matrix **C** such that the coincidence rate per unit of volume can be written as:

$$N(\hat{\varepsilon}) = \hat{\varepsilon}^* \cdot \mathbf{C} \cdot \hat{\varepsilon}. \tag{3.2}$$

The polarization matrix **C** determines the intensity and polarization of photons emitted in any direction, and is therefore particularly suited for the study of the effects of a finite interaction region.

Because the **C** matrix is related to the density matrix of the excited atoms, any anisotropy of the excited state density matrix will result in a similar anisotropy of the intensity and polarization of the emitted radiation. The exact relation between ρ_i and **C** can be found by expanding both ρ_i and **C** in irreducible spherical tensors.

A general expression for **C** can be found by applying Hermiticity of ρ_i and reflection symmetry of ρ_i with respect to the scattering plane. Nienhuis (1980) (see also Beijers

et al 1987) has shown that **C** is given by:

$$\mathbf{C}=\frac{I_z}{2}\begin{pmatrix} 1+P_1 & P_2+\mathrm{i}P_3 & 0 \\ P_2-\mathrm{i}P_3 & 1-P_1 & 0 \\ 0 & 0 & C_{33} \end{pmatrix} \tag{3.3}$$

where

$$C_{33}=\frac{(1+P_1)(1-P_4)}{(1+P_4)}. \tag{3.4}$$

Here I_z is the coincidence rate for the radiation emitted in the z-direction, P_1, P_2, and P_3 are the Stokes parameters of the radiation emitted in the z-direction, and P_4 is the linear polarization of the radiation emitted in the $+y$ (or $-y$) direction. The **C** matrix is here given with respect to the natural coordinate frame, and a classical definition of P_3 is used (see equation (2.20) of Andersen *et al* 1988). The form of the **C** matrix as given in (3.3) holds for any atomic dipole transition, assuming that the incident electrons and the atoms in the initial state are unpolarized, and that the spin of the scattered electron is unobserved.

Two specific situations are relevant with regard to the results presented in this paper.

(i) He(n^1P) excitation. For the atom *LS* coupling is valid and the influence of the spin–orbit interaction during the collision is negligible. The excitation process is fully coherent and it can be derived that $C_{33}=0$ and:

$$\begin{aligned} &P_1^2+P_2^2+P_3^2=1 \\ &P_4=1. \end{aligned} \tag{3.5}$$

In this case the excited atom is fully described by P_1, P_2 and the sign of P_3.

(ii) Excitation of the $ns'[\frac{1}{2}]_1^0$ and $ns[\frac{3}{2}]_1^0$ resonance transitions in the noble-gas atoms. For the noble-gas atoms the spin–orbit effects may be so strong that spin-flip can occur during the collision. Contributions from the scattering of spin-up and spin-down electrons add incoherently. In this case it follows that (Andersen *et al* 1988):

$$\begin{aligned} &P_1^2+P_2^2+P_3^2\leqslant 1 \\ &P_4\leqslant 1. \end{aligned} \tag{3.6}$$

The $P_{1,2,3}$ parameters refer to excitation with positive reflection symmetry in the scattering plane. The P_4 parameter is related to ρ_{00} (see equation (3.7) below) referring to an excitation mechanism with negative reflection symmetry involving (*a*) spin-flip due to spin–orbit interaction during the collision, and/or (*b*) exchange with an atomic electron of opposite spin.

Based on the density matrix for an excited atom in a P state, Andersen *et al* (1986, 1988) derived an angular charge density distribution ('charge cloud'), and introduced the following physically insightful parameters:

$$\begin{aligned} &P_l^+\,\mathrm{e}^{2\mathrm{i}\gamma}=P_1+\mathrm{i}P_2 \\ &L_\perp^+=-P_3 \\ &\rho_{00}=\frac{(1+P_1)(1-P_4)}{4-(1-P_1)(1-P_4)} \end{aligned} \tag{3.7}$$

where P_l^+ is the linear polarization of the charge density distribution in the collision plane, γ is the alignment angle indicating the alignment of the charge density distribution in the scattering plane, $L_\perp^+$ is the angular momentum expectation value for the part of the density matrix with positive reflection symmetry, and ρ_{00} is the height parameter of the charge density distribution.

In the experiment described in this paper the coherence parameters are obtained from an analysis of the polarization of the emitted photons. In equation (3.1) an ideal situation is assumed in the sense that the photon detector is sensitive to light with a particular polarization $\hat{\varepsilon}$ only. It is convenient to generalize equation (3.1) for a detector with arbitrary polarization sensitivity. Using a right-handed orthogonal set of unit vector $\{\hat{\varepsilon}_1, \hat{\varepsilon}_2, \hat{n}\}$ the 2×2 density matrix for the photons emitted in the direction $\hat{n} = (\sin\theta\cos\phi, \sin\theta\sin\phi, \cos\theta)$ has the elements:

$$c_{ij} = \hat{\varepsilon}_i \cdot \mathbf{C} \cdot \hat{\varepsilon}_j. \tag{3.8}$$

The density matrix is here given with respect to the linear polarization vectors $\hat{\varepsilon}_1$ and $\hat{\varepsilon}_2$, and is known in optics as the coherency matrix (O'Neill 1963). It can be expressed in terms of the Stokes parameters $P_1(\hat{n})$, $P_2(\hat{n})$ and $P_3(\hat{n})$ of the light emitted in the direction $\hat{n}$:

$$\mathbf{c} = \frac{1}{2}\begin{pmatrix} 1+P_1(\hat{n}) & P_2(\hat{n})+iP_3(\hat{n}) \\ P_2(\hat{n})-iP_3(\hat{n}) & 1-P_1(\hat{n}) \end{pmatrix}. \tag{3.9}$$

According to the coherency matrix formalism the transformation law for the density (coherency) matrix for light passing through an optical component is (see O'Neill 1963):

$$\mathbf{c}' = \mathbf{A}\mathbf{c}\mathbf{A}^\dagger \tag{3.10}$$

where $\mathbf{A}$ is the Jones matrix representing the operation of the optical component. Introducing a 2×2 efficiency matrix $\mathbf{E}$ for the photon detector behind the optical component the detected signal follows from

$$\begin{aligned} I &= \mathrm{Tr}(\mathbf{E}\mathbf{c}') \\ &= \mathrm{Tr}(\mathbf{E}\mathbf{A}\mathbf{c}\mathbf{A}^\dagger). \end{aligned} \tag{3.11}$$

In most optical systems used in coherence experiments (see Slevin and Chwirot 1990) the Stokes parameters are extracted from a measurement of the detected signal as a function of the angle of one or more rotatable optical components. The present experiment uses single and double-reflection polarization analysers (Westerveld *et al* 1985) that employs reflection from gold coated mirrors.

3.3. Numerical model

We have developed a computer program to numerically simulate the effect of a finite interaction region on the measured Stokes parameters. In the model the finite volume of the intersection of the electron beam and the gas jet is represented by an array of discrete scattering points. For each point the intensity of the light detected by either the channeltron perpendicular to the nominal scattering plane or the channeltron in the nominal scattering plane is calculated. The total signals are obtained by summing over all the array points.

For every array point in the interaction region the calculation proceeds through the following steps:

(1) Calculation of the set of unit vectors $\hat{b}_1$, $\hat{b}_2$, and $\hat{b}_3$ for the $\{x', y', z'\}$ coordinate frame. For a particular array point the scattering plane is defined by the direction $\hat{b}_1$ of the incident electron and the direction $\hat{n}_s$ of the scattered electron passing through the entrance aperture of the electron energy analyser, as illustrated in figure 2. The vectors $\hat{b}_2$ and $\hat{b}_3$ can be obtained by:

$$\hat{b}_3 = \frac{\hat{b}_1 \times \hat{n}_s}{|\hat{b}_1 \times \hat{n}_s|} \qquad \hat{b}_2 = \hat{b}_3 \times \hat{b}_1. \tag{3.12}$$

(2) Evaluation of the scattering angle (angle between $\hat{b}_1$ and $\hat{n}_s$) and the corresponding theoretical Stokes parameters. The theoretical Stokes parameters are found by interpolation on the tabulated results from Bartschat and Madison (1987) for the noble-gas atoms, and from Madison and Winters (1983) for helium. The theoretical Stokes parameters determine the polarization matrix $\tilde{C}$, identical to equation (3.3) but here in reference to the $\{x', y', z'\}$ coordinate frame:

$$\tilde{C} = \frac{\tilde{I}_z}{2}\begin{pmatrix} 1+\tilde{P}_1 & \tilde{P}_2+i\tilde{P}_3 & 0 \\ \tilde{P}_2-i\tilde{P}_3 & 1-\tilde{P}_1 & 0 \\ 0 & 0 & \tilde{C}_{33} \end{pmatrix} \tag{3.13}$$

where $\tilde{P}_i$ denote the theoretical Stokes parameters in reference to the $\{x', y', z'\}$ frame.

(3) Calculation of the radiation pattern in the lab frame by transformation of the $\tilde{\mathbf{C}}$ matrix given by equation (3.13) from the $\{x', y', z'\}$ frame to the $\{x, y, z\}$ frame (laboratory frame). This is performed by using:

$$\mathbf{C} = \mathbf{R}^{\dagger}\tilde{\mathbf{C}}\mathbf{R} \tag{3.14}$$

where the elements of the rotation matrix $\mathbf{R}$ are given by the components of the unit vectors $\hat{b}_1$, $\hat{b}_2$, and $\hat{b}_3$ with respect to the $\{\hat{a}_1, \hat{a}_2, \hat{a}_3\}$ basis set, i.e.

$$R_{ij} = \hat{b}_i \cdot \hat{a}_j. \tag{3.15}$$

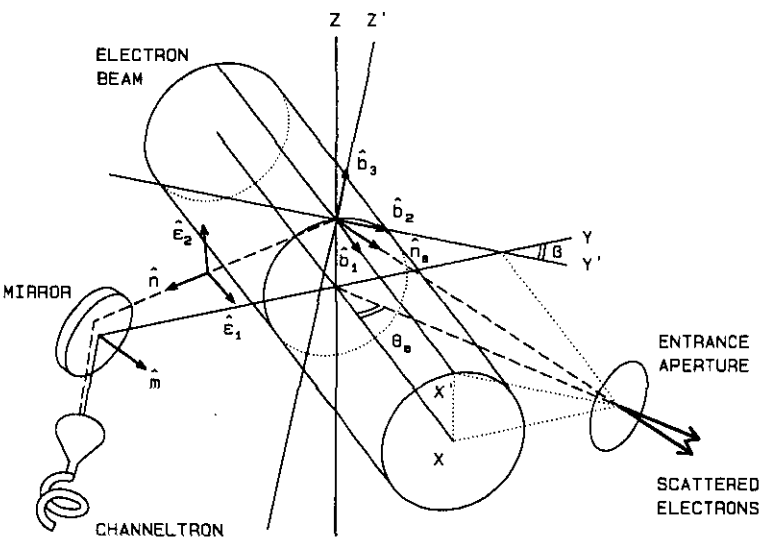

Figure 2. Schematic diagram illustrating the various vectors and other parameters relevant to the numerical model (section 3.3).

(4) Calculation of the Stokes parameters for the radiation emitted towards the photon detectors perpendicular to and in the nominal collision plane. The photon detector in the nominal collision plane is at a variable angle θ_4 with respect to the electron beam, the value of which can be set to 90°, 45°, or any other angle in the program. The 2×2 density matrix $\mathbf{c}$, specifying the Stokes parameters for the radiation emitted in direction $\hat{n}$, can be obtained from equation (3.8).

(5) Calculation of the intensity of the radiation detected by the photon detector in the nominal scattering plane. In order to obtain the intensity from equation (3.11) the optical components in the detector need to be taken into account. For a reflecting surface as employed in our detectors, the Jones matrix takes the form (Westerveld *et al* 1985):

$$\mathbf{A}=\begin{pmatrix} r_p \exp i\delta_p & 0 \\ 0 & r_s \exp i\delta_s \end{pmatrix}. \tag{3.16}$$

Here $r_p \exp i\delta_p$ and $r_s \exp i\delta_s$ are the complex reflection coefficients for light polarized parallel and perpendicular to the plane of reflection, respectively. For reflection from a flat surface the reflection coefficients can be expressed in terms of the complex index of refraction of the surface medium. The mirrors used in our experiment are gold coated, and the angle of incidence is chosen such that $\cos(\delta_p-\delta_s)=0$. Assuming that the photon detector is insensitive to polarization and has an efficiency e_0 for the total intensity of the incident radiation, the detected signal becomes:

$$I(\alpha)=e_0\sum_{ijk} A_{ki}\hat{\varepsilon}_i\cdot\mathbf{C}\cdot\hat{\varepsilon}_j A^*_{kj}. \tag{3.17}$$

Here α is the angle between the reflection plane and the nominal scattering plane (either 0 or $\pi/2$). As discussed in section 2 the linear polarization is obtained from measurements of the intensity with the mirror reflecting in the scattering plane and out of the scattering plane. To apply this equation the vectors $\hat{\varepsilon}_1$ and $\hat{\varepsilon}_2$ are chosen parallel and perpendicular to the reflection plane defined by the unit vectors $\hat{n}$ and $\hat{m}$ (normal vector of the mirror), figure 2. The linear polarization in the nominal scattering plane is obtained from:

$$P_4^{\mathrm{M}}(\theta_4)=\sum\frac{I(0°)-I(90°)}{I(0°)+I(90°)} \tag{3.18}$$

where the summation is over the array of scattering points in the interaction region.

(6) Calculation of the intensity of the radiation detected by the photon detector perpendicular to the nominal scattering plane. A similar method could be used for the signal obtained by this detector. However, in our calculations the measured Stokes parameter P_1^M is obtained directly from the 2×2 x-y submatrix of $\mathbf{C}$ in equation (3.14):

$$P_1^M=\sum\frac{C_{11}-C_{22}}{C_{11}+C_{22}}. \tag{3.19}$$

This amounts to assuming that only radiation emitted parallel to the z-axis from every array point in the interaction region is detected. This is a legitimate approximation in view of the large distance (about 120 mm) of the detector from the interaction region.

In these calculations the array of discrete scattering points is generated in the following manner. We start out with a three-dimensional equidistant array of points (cubic lattice) with the distance between adjacent array points to be set by the user of the program. The finite size of the electron beam is modelled by rejecting all array

points outside the radius of the electron beam. Apart from the radius, the displacement position of the beam axis in the $y-z$ plane can be specified in the program. In addition a divergent (or convergent) electron beam can be modelled by deforming the lattice of array points towards a focal point of the electron beam specified by the user.

The finite size and density of the gas jet are implemented by assigning a weight factor to each array point. We use two density models for the gas flow out of the single capillary tube.

(i) Cone model. The gas flow is assumed to have a cone shape of which the top angle can be specified. Array points within the cone are assigned a weight proportional to the inverse square of the distance of the array point to the exit of the tube. Array points outside the cone are rejected.

(ii) Model of Olander and Kruger (1970). For gas flow through a single capillary tube Olander and Kruger (1970) show that

$$n(x, y, z) = \frac{\dot{N}}{vK} \frac{j(\alpha)}{\pi r^2} \tag{3.20}$$

where $\dot{N}$ is the total flow rate (number of particles per second) through the tube, $v = \sqrt{3kT/M}$ is the average thermal velocity of particles in the beam, $j(\alpha)$ is a normalized distribution function that depends on the flow conditions in the tube, α is the angle between the direction to the array point and the centreline of the tube, r is the distance from the tube exit to the array point, and K is the transmission probability (Clausing factor) of the tube. Array points are assigned a weight proportional to the density given by this equation.

A second weight factor is introduced to account for the variation of the differential cross section. For the noble gases the differential cross section often decreases over several orders of magnitude when the scattering angle increases from 0–30°. Within the small range of scattering angles accepted by the analyser the smaller angles will be slightly favoured. This effect was found to be significant in the forward scattering studies of Martus *et al* (1988).

The finite acceptance angles of the P_4 channeltron and electron energy analyser are implemented in the program as options. Effects due to these are calculated by choosing a few grid points within the radius of the channeltron cone or within the radius of the entrance aperture of the electron energy analyser. For each array point the signals are obtained by adding the intensities calculated individually for each grid point. Variation in the transmission function of the electron analyser is taken into account by assuming that this function is triangular in shape.

In summary the following effects can be simulated with our program:

(i) the finite radius, displacement, and convergence/divergence of the electron beam,

(ii) the finite dimension, displacement and density profile of the gas jet,

(ii) the variation of the Stokes parameters and the differential cross section as a function of the scattering angle within the interaction region,

(iv) the optical properties and finite acceptance angle of the P_4 photon detector, and

(v) the finite acceptance angle of the electron energy analyser.

3.4. Approximate analytical model

The numerical model discussed in the previous section requires detailed information in the form of the Stokes parameters as a function of scattering angle. It is therefore

not usable for the correction of measured Stokes parameters, unless some functional dependence of the Stokes parameters with scattering angle is assumed, or a great many experimental data points for many scattering angles are measured. In this section we derive analytical expressions for the measured Stokes prameters, based on the assumption that only the finite size of the electron beam is important for the effects of a finite interaction region. The analytical expressions are suitable for correction of experimental data (discussed in more detail by Corr *et al* 1991) and provide a qualitative insight into the effect of a finite interaction region.

The analytical model ignores the variation of the Stokes parameters over the small range of scattering angles within the interaction region. It assumes that the opening angle of the photon detectors and of the entrance aperture of the analyser are of minor importance. The model applies to a parallel electron beam only. Despite these approximations we have found that, in comparison with the numerical model, the analytical model gives very reasonable results.

We take another look at figure 1. For electrons scattered from a point with coordinates $(0, y_p, z_p)$ off the centre of the electron beam the collision plane is defined by the x' and y' axes, (as illustrated in figure 1 for a point at the top of the electron beam). For this point the polarization matrix $\tilde{\mathbf{C}}$ with respect to the $\{x', y', z'\}$ coordinate frame is given by equation (3.13):

As the scattered electrons pass through the first aperture in the electron energy analyser, at a distance R_e from the scattering centre, the $\{x', y', z'\}$ frame is rotated with respect to the $\{x, y, z\}$ frame over an angle β around an axis parallel to the x-axis.

$$\tan\beta = \frac{z_p}{R - y_p} = \frac{z_p}{R_e \sin\theta_e - y_p} \tag{3.21}$$

where θ_e is the scattering angle. The polarization matrix with respect to the $\{x, y, z\}$ frame can now be found by using the rotation matrix for a rotation over β about the x-axis:

$$\mathbf{R}(\beta) = \begin{pmatrix} 1 & 0 & 0 \\ 0 & \cos\beta & -\sin\beta \\ 0 & \sin\beta & \cos\beta \end{pmatrix} \tag{3.22}$$

so that:

$$\mathbf{C}(\beta) = \mathbf{R}^{\dagger}(\beta)\tilde{\mathbf{C}}\mathbf{R}(\beta). \tag{3.23}$$

If we now assume that the radiation from individual atoms excited at various points in the interaction region adds incoherently, we can derive the intensity and polarization of the emitted radiation from all excited atoms in the interaction region by integrating (or averaging) $\mathbf{C}(\beta)$ over the interaction region. This approach is justified because the distance to the photon detectors is much larger than the size of the interaction region. Assuming (as discussed above) that the variation of the scattering angle for points within the interaction region is negligible, we can restrict the averaging to points located in the $y-z$ plane within the electron beam radius r. It follows that $\overline{\sin\beta} = 0$, $\overline{\sin\beta\cos\beta} = 0$, and as a result:

$$\bar{C} \sim \begin{pmatrix} 1+P_1 & (P_2+\mathrm{i}P_3)\,\overline{\cos\beta} & 0 \\ (P_2-\mathrm{i}P_3)\,\overline{\cos\beta} & (1-P_1)\,\overline{\cos^2\beta} + C_{33}\,\overline{\sin^2\beta} & 0 \\ 0 & 0 & (1-P_1)\,\overline{\sin^2\beta} + C_{33}\,\overline{\cos^2\beta} \end{pmatrix} \tag{3.24}$$

where

$$\overline{\sin^2\beta} = \frac{r^2}{4R^2}$$

$$\overline{\cos^2\beta} = 1 - \frac{r^2}{4R^2} \tag{3.25}$$

$$\overline{\cos\beta} \approx \frac{4R}{r} + \frac{2R^2}{r(r+R)} - \frac{6R^2}{r^2}\ln\frac{R+r}{R}.$$

Ignoring the opening angle of the photon detectors by assuming that all detected radiation is emitted parallel to the z-axis it follows that the polarization is described by the 2×2 $x-y$ submatrix of **C**. The measured P_1^{M} parameter becomes:

$$P_1^M = \frac{1 - \left(\frac{1-P_1}{1+P_1}\right)\overline{\cos^2\beta} - \left(\frac{1-P_4}{1+P_4}\right)\overline{\sin^2\beta}}{1 + \left(\frac{1-P_1}{1+P_1}\right)\overline{\cos^2\beta} + \left(\frac{1-P_4}{1+P_4}\right)\overline{\sin^2\beta}}. \tag{3.26}$$

Similar expressions are obtained for the measured P_2^{M} and P_3^{M} parameters. Analogously the measured P_4^M parameter can be found from the $x-z$ submatrix of **C**:

$$P_4^{\mathrm{M}} = \frac{1 - \left(\frac{1-P_1}{1+P_1}\right)\overline{\sin^2\beta} - \left(\frac{1-P_4}{1+P_4}\right)\overline{\cos^2\beta}}{1 + \left(\frac{1-P_1}{1+P_1}\right)\overline{\sin^2\beta} + \left(\frac{1-P_4}{1+P_4}\right)\overline{\cos^2\beta}}. \tag{3.27}$$

In the case of helium $P_4 = 1$ and equation (3.27) reduces to:

$$P_4^M = \frac{1 - \left(\frac{1-P_1}{1+P_1}\right)\overline{\sin^2\beta}}{1 + \left(\frac{1-P_1}{1+P_1}\right)\overline{\sin^2\beta}}. \tag{3.28}$$

With regard to spurious effects on P_4^{M} due to a finite interaction region, equation (3.27) illustrates two important points. First, since the effect depends on $\overline{\sin^2\beta}$, it is only likely to be significant for small scattering angles where the variation of β is the largest. Second, an amplifying effect occurs for $P_1 < 0$, especially when P_1 approaches -1. For excitation of the noble-gas atoms at intermediate energies P_1 becomes negative at small scattering angles, where the variation of β can become significant, and where part of our measurements are being carried out. Thus, in a graphical picture, an effect on P_4^{M} is expected for small scattering angles, especially if the charge cloud is very elongated and at those angles where the charge cloud is facing the P_4 photon detector end on.

Clearly, from equation (3.26) we expect a much smaller effect on P_1^{M}, because for the noble-gas atoms P_4 is anticipated to be close to unity over the full range of scattering angles.

We finally note that the equations (3.26) and (3.27) can easily be inverted, resulting in expressions for P_1 and P_4 in terms of P_1^{M} and P_4^{M} that can be used to correct experimental data (see Corr *et al* 1991).

4. Results and discussion

In this section we present data to illustrate the magnitude of the effects outlined earlier. For the sake of clarity we will take one data set which we assume to be accurate and then we will investigate how this data set is modified by the inclusion of these experimental effects. We assume the calculated data set of Bartschat and Madison (1987). In all the figures presented this data set is shown as a full curve. The modified data are give as separate data points. The data all pertain to $I = 0$ isotopes. We chose Ar as the optimum test gas because it satisfies this restriction on nuclear spin. In the calculations the diameter of the entrance aperture of the electron energy analyser was taken as 1 mm. R_e (figure 1) was 28.5 mm.

Figure 3 shows the four Stokes parameters for Ar $4s'[\frac{1}{2}]_1^0$ at 80 eV incident energy and a range of electron scattering angles from 0–30°. Here the analytical model is used for a beam radius of 1 mm and a 1 mm vertical displacement of the beam out of the nominal scattering plane. It is clear from figure 3 that $P_{1,2,3}$ are affected in a very minor way but a serious perturbation of the P_4 data is evident. This is largely due to the magnifying effect of a P_1 which is large and negative, equation (3.27). Since $P_4 = 1$ in the primary data set it is clear from equation (3.26) that modifications to $P_{1,2,3}$ will only occur at small θ_e where $\cos^2 \beta$ diverges significantly from unity. We note that Simon *et al* (1990) also found significant interaction volume effects at small electron scattering angles, (less than 6°).

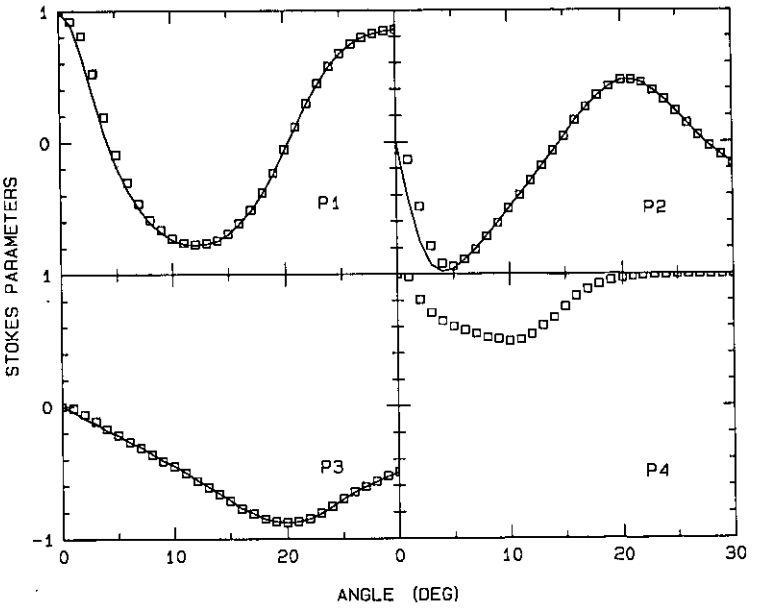

Figure 3. Stokes parameters for excitation of Ar $4s'[\frac{1}{2}]_1^0$ by 80 eV electrons as a function of electron scattering angle. The full curves indicate the DWBA data of Bartschat and Madison (1987). Note that for P_4 this coincides with $P_4 = 1$ at all angles. The squares are data calculated using the analytical model (section 3.4) assuming an electron beam of radius 1 mm and a 1 mm vertical offset of the beam out of the nominal scattering plane. We note that a modified version of equation (3.27) is used in this calculation to take account of this offset.

Figure 4 again presents P_1 and P_4 data for 80 eV excitation of Ar but this time modified data are presented for the two models (analytical and numerical) discussed earlier in the text. The assumed beam radius and offset are the same as in figure 3. Very little effect is seen for the P_1 data; some small differences between the two models are evident in the P_4 data though both models show similar large divergences from the original data set at $\theta_e < 20°$.

Figure 5 is a further presentation of 80 eV Ar data only now the beam radius has been increased to 2 mm and the 1 mm vertical offset assumed in figures 3 and 4 has been eliminated. A remarkable similarity between the modified data sets of figures 4 and 5 is evident indicating the need for careful focusing of the electron beam when the coincidence measurements are attempted for small electron scattering angles.

Figure 6 shows the effect of misalignment of the electron beam *in* the scattering plane. The modified data shown refer to an electron beam of 1 mm radius but now offset by 1 mm from the nominal scattering centre in the scattering plane. As might be expected a more significant effect than before is observed in the P_1 data with a smaller but still significant effect apparent in the P_4 data. An effect of the same magnitude is observed in the P_4 data if no offset of the electron beam is assumed. Figure 6 thus shows the effect on P_4 of finite electron beam radius (1 mm) alone.

Figure 7 illustrates the effect of a lack of parallelism of the electron beam as it passes through the interaction region. Figure 7 shows the range of θ_e where this effect could be significant.

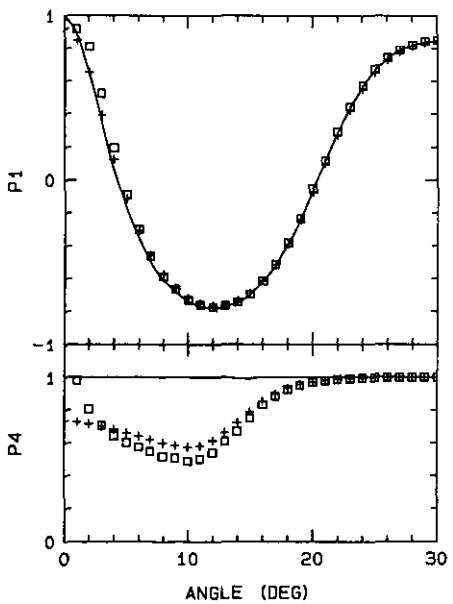

Figure 4. P_1 and P_4 data for excitation of Ar $4s'[\frac{1}{2}]^1_0$ by 80 eV electrons. Full curves, Bartschat and Madison (1987), DWBA calculation; squares, approximate analytical model (section 3.4); crosses, numerical model, (section 3.3). For both models a 1 mm electron beam radius and a vertical offset out of the scattering plane of 1 mm have been assumed.

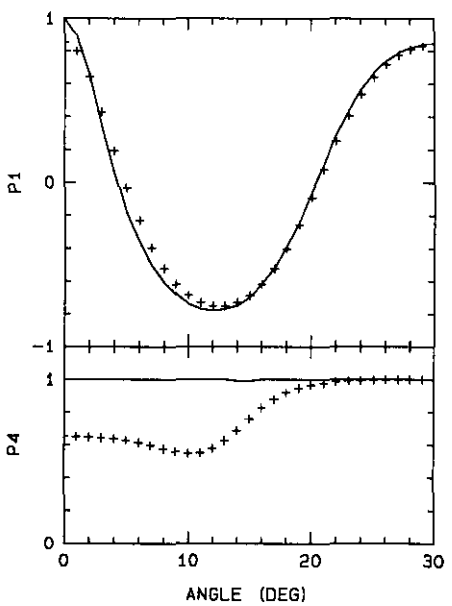

Figure 5. P_1 and P_4 data for excitation of Ar $4s'[\frac{1}{2}]^0_1$ by 80 eV electrons. Symbols as in figure 4. The crosses refer to data modelled assuming a beam radius of 2 mm. No displacement of the beam from its nominal position is assumed.

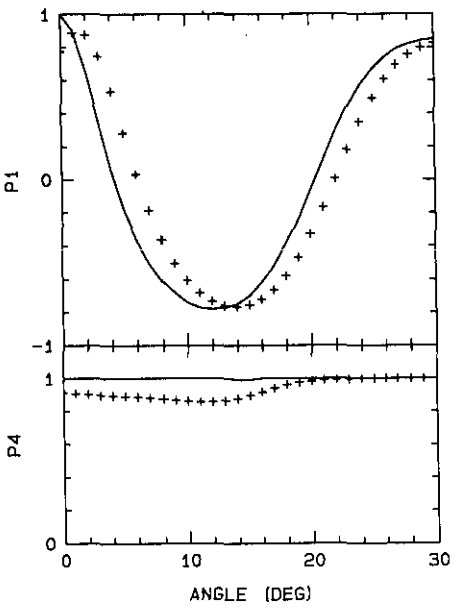

Figure 6. P_1 and P_4 data for excitation of Ar $4s'[\frac{1}{2}]_1^0$ by 80 eV electrons. Symbols as in figure 4. The crosses refer to data modelled assuming a 1 mm beam radius and a horizontal displacement of the electron beam of 1 mm in the scattering plane.

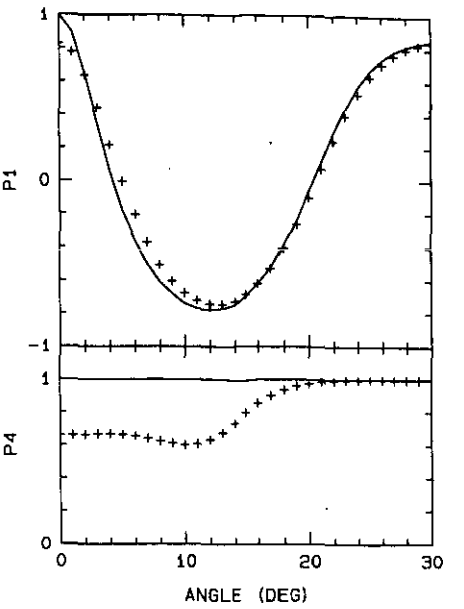

Figure 7. P_1 and P_4 data for excitation of Ar $4s'[\frac{1}{2}]_1^0$ by 80 eV electrons. Symbols as in figure 4. The crosses refer to data modelled assuming an electron beam of 1 mm radius at the scattering centre but diverging from a point 40 mm from this centre. No displacement of the beam from its nominal axis is assumed.

In the calculations mentioned above we chose realistic values for the parameters of the gas jet using the Olander and Kruger model. Within reasonable limits on these parameters we observed very little effect on the Stokes parameters indicating that the position and density profile of the gas jet are not critical. Additional calculations using the simpler 'cone' model (section 3.3) gave very similar results. As an experimental check on this we carried out measurements using two different gas inlet systems (see Corr *et al* 1991) with identical results. Other factors which were considered and which only showed very minor effects were the finite acceptance angles of the photon and electron detectors and the possible variation of the optical properties of the photon detectors as they were rotated. This is not unexpected in our case because of the relatively large distances to the detectors. If however the acceptance angles of the detectors are relatively large, proper allowance must be made for this as was done for example by Beijers (1987) or Anderson (private communication, 1989). In all cases we took account of the variation of the Stokes parameters and the differential cross section as a function of the electron scattering angle within the interaction region. This was only found to be significant in regions where the Stokes parameters varied rapidly with θ_e, for example close to $\theta_e = 0$. In this region our modified data are consistent with those of Martus *et al* (1988).

It is clear from these calculations that significant apparent departues of P_4 from unity could be obtained if electron beam focusing and alignment are not carefully controlled. Previously (see McConkey *et al* 1989), we attributed such a variation of P_4 from unity in our measurements with Kr targets to just these effects. It is now clear (Corr *et al* 1991) that internal atomic interactions were the cause of the anomalous

measured data. These can result in serious depolarizing effects which can have a much more dramatic effect on P_4 than any of the experimental problems discussed so far. Section 5 presents a discussion of these effects.

Clearly the best way to check a system for the presence of finite interaction volume effects is to use a target like Ar (or Ne) which is free from perturbing internal interactions. Any divergence of P_4 from unity for these targets in the angular range where P_1 is large and negative ($\gamma \approx \pi/2$) could be taken as an indication of the existence of some of the effects discussed. An example of a set of these measurements for our coincidence machine is given in figure 8 where 80 eV excitation of Ar is displayed. Clearly P_4 is not significantly different from unity in the important region of θ_e. Similar results were obtained for Ne (see Corr *et al* 1991). An additional test which we found gave a good indication of the proper alignment of the system was to measure the non-coincident photon signal in the P_1 and P_4 detectors as they were rotated through their full angular range. Asymmetries in the system were readily detected as asymmetries in the signals from the 0°–180°, 90°–270° detector positions.

If it is found impossible to get rid of finite volume effects then the only alternative is to include a further polarization analyser in the scattering plane, say at 45° to the incident electron beam. This could then be used for electron scattering angles where the charge cloud had rotated to the position where it was orthogonal to the exciting electron beam and faced the original P_4 detector 'end-on'.

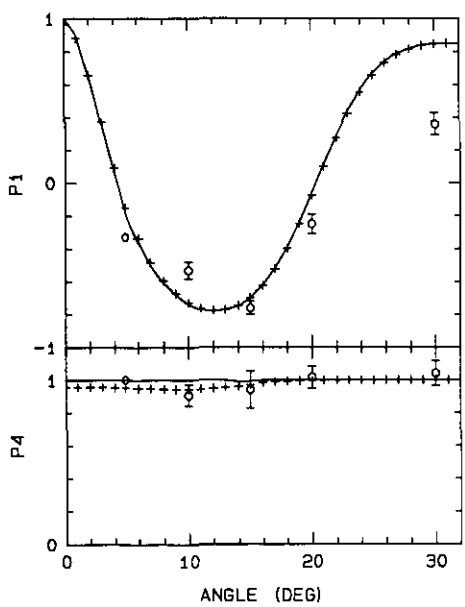

Figure 8. Comparison of experimental and calculated P_1 and P_4 data for excitation of Ar $4s'[\frac{1}{2}]_1^0$ by 80 eV electrons. Circles with error bars, experimental data of Corr *et al* (1991). Other symbols as in figure 4. The crosses refer to data modelled assuming a parallel electron beam of radius 0.5 mm and no displacement of the scattering centre from its nominal position. These parameters are chosen to reflect as accurately as possible the actual experimental parameters.

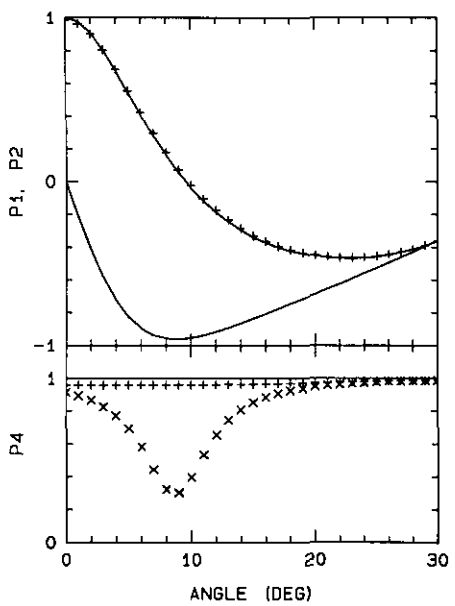

Figure 9. P_1, P_2 and P_4 data for excitation of He 2^1P by 80 eV electrons illustrating the effect of using different P_4 detector positions. Full curves, DWBA calculations of Madison and Winters (1983); + and ×, data modelled for in plane photon detector at 90° and 45° respectively to the electron beam direction. Modelled data refer to a parallel electron beam of 1 mm radius which passes through the nominal scattering centre. Note how the large dip in P_4 (45°) coincides with the deep minimum in P_2.

As a note of caution, however, we should point out that if such a detector is used then serious instrumental effects might be expected when P_2 (rather than P_1) is large and negative. This occurs even for He under certain scattering conditions as is illustrated in figure 9. Figure 9 shows that although these finite interaction volume effects are very small for a conventionally placed P_4 detector, they could be quite severe for one positioned at 45° to the incident beam.

5. Depolarization due to internal atomic interactions

As discussed in detail by Andersen *et al* (1988) and others, it is often possible for depolarization to occur following the initial excitation due to fine or hyperfine interactions which take effect prior to the radiative decay of the state. In the heavy rare gases where the individual fine-structure states can be isolated in the electron channel this interaction is not a problem. However in some cases hyperfine depolarization can be serious. This is illustrated in the cases of Kr and Xe in the following paper (Corr *et al* 1991) and so the necessary analysis is provided here.

The depolarizing effect of the hyperfine interaction can be studied using the formalism of Nienhuis (1980). We briefly summarize the results. The effect is described by introducing the reduction factors G_k (denoted r_k by Nienhuis 1980). For the case that the lifetime is very much longer than the hyperfine interaction time (and fine structure is resolved) the reduction factors are:

$$G_k = \sum_F \frac{(2F+1)^2}{2I+1} \begin{Bmatrix} F & F & k \\ J & J & I \end{Bmatrix}^2 \qquad (5.1)$$

$$G_0 = 1.$$

Nienhuis (1980) has shown that the effect of hyperfine interaction on the polarization matrix **C** is found by simply multiplying the multipole components c_{kq} of the **C** matrix by G_k (see also Beijers *et al* 1987). One finds that **C** is given by:

$$\mathbf{C} = \begin{pmatrix} \frac{1}{\sqrt{3}} c_{00} + \frac{G_2}{\sqrt{6}} c_{20} - \frac{1}{2} G_2(c_{22}+c_{2-2}) & G_1 \frac{-\mathrm{i}}{\sqrt{2}} c_{10} + \frac{\mathrm{i}}{2} G_2(c_{22}-c_{2-2}) & 0 \\ G_1 \frac{i}{\sqrt{2}} c_{10} + \frac{i}{2} G_2(c_{22}-c_{2-2}) & \frac{1}{\sqrt{3}} c_{00} + \frac{G_2}{\sqrt{6}} c_{20} + \frac{1}{2} G_2(c_{22}+c_{2-2}) & 0 \\ 0 & 0 & \frac{1}{\sqrt{3}} c_{00} - G_2 \sqrt{\frac{2}{3}} c_{20} \end{pmatrix}. \qquad (5.2)$$

Comparing this equation with equation (3.3) one can derive the time-averaged Stokes parameters P_i' in terms of the Stokes parameters P_i which would occur in the absence of hyperfine interaction:

$$P_1' = \frac{3G_2(1-\rho_{00})}{2+G_2(1-3\rho_{00})} P_1 \qquad (5.3)$$

$$P_2' = \frac{3G_2(1-\rho_{00})}{2+G_2(1-3\rho_{00})} P_2 \qquad (5.4)$$

$$P_3' = \frac{3G_1(1-\rho_{00})}{2+G_2(1-3\rho_{00})} P_3 \qquad (5.5)$$

$$P_4' = \frac{G_2(1-3\rho_{00}) + G_2(1-\rho_{00})P_1}{\frac{4}{3} - \frac{1}{3}G_2(1-3\rho_{00}) + G_2(1-\rho_{00})P_1}. \qquad (5.6)$$

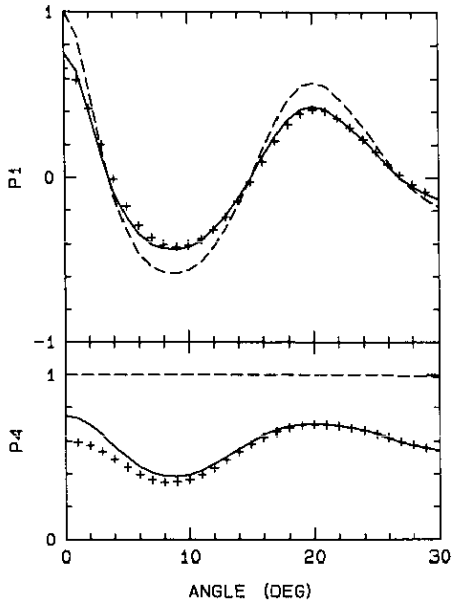

Figure 10. P_1 and P_4 data for excitation of Xe $6s[\frac{3}{2}]_1^0$ by 80 eV electrons. Broken curve, data of Bartschat and Madison (1987); full curve, same data but corrected for hyperfine depolarization effects; crosses, data corrected for both hyperfine depolarization and finite interaction volume effects. The crosses refer to data modelled assuming a parallel electron beam of 1 mm radius which passes through the scattering centre.

We note that equations (5.3)–(5.5) are equivalent to equations C.33–C.36 of Anderson *et al* (1988).

Figure 10, which presents comparative data for 80 eV excitation of Xe$6s[\frac{3}{2}]_1^0$, illustates the significant depolarizing effect which can occur due to hyperfine interactions. Here the time-averaged Stokes parameters, obtained from equations (5.3)–(5.6) were used in the modelling of the effect of a finite interaction region. In this situation the effects of a finite interaction region are clearly minor as compared to the hyperfine depolarization.

6. Conclusions

We have developed models to investigate a number of effects which arise due to the finite volume of the interaction region and the finite acceptance angles of the electron and photon detectors. The effects can be particularly severe in the measurement of the P_4 coherence parameter. Slight misalignment or defocussing of the electron beam through the nominal scattering centre can have dramatic effects on the measured P_4 particularly at small scattering angles and when $P_1 \ll 0$. It is suggested that the use of Ne or Ar as target species can help identify the magnitude of any effect which might be present. Non-coincident polarization measurements provide a sensitive method for checking system alignment. In some cases placing the in-plane detector at $\pi/4$ to the beam direction can be helpful.

When any internal atomic depolarizing interaction is occurring so that the charge cloud acquires a 'height', the effect on P_4 measurements is much greater than any of

the finite interaction region effects which were investigated. This is further illustrated in the companion paper by Corr *et al* (1991).

We note finally that effects due to a finite interaction region might also be expected to play a role in so-called angular-correlation experiments where the radiation pattern is probed by moving the photon detector in the scattering plane or in another plane inclined to this.

Acknowledgments

The financial assistance of the Natural Sciences and Eingineering Research Council of Canada, NATO Division of Scientific Affairs (RG 686/84) and the Killam Foundation is gratefully recognized. Helpful discussion with N Anderson, K Barschat, G Csanak, D K Madison, S Trajmar and P W Zetner are gratefully acknowledged. The authors are indebted to K Bartschat and D K Madison for extensive tabulations of their published data.

References

Andersen N, Gallagher J W and Hertel I V 1986 *Proc. 14th Int. Conf. on the Physics of Electronic and Atomic Collisions (Palo Alto)* ed D C Lorents, W E Meyerhof and J R Peterson (Amsterdam: North Holland) Invited Papers pp 57-76

Andersen N, Gallagher J W and Hertel I V 1988 *Phys. Rep.* **165** 1-188

Bartschat K and Madison D H 1987 *J. Phys. B: At. Mol. Phys.* **20** 5839-63

Beijers J P M 1987 *PhD Thesis* University of Utrecht, The Netherlands

Beijers J P M, Doornenbal S J, van Eck J and Heideman H G M 1987 *J. Phys. B: At. Mol. Phys.* **20** 5529-40

Corr J J, van der Burgt P J M, Plessis P, Khakoo M A, Hammond P and McConkey J W 1991 *J. Phys. B: At. Mol. Opt. Phys.* **24** 1069-85

Danjo A, Koike T, Kani K, Sugahara H, Takahashi A and Nishimura H 1985 *J. Phys. B: At. Mol. Phys.* **18** L595-600

da Paxiao F J, Padial N T and Csanak G 1984 *Phys. Rev.* A **30** 1697-713

Hanne G F 1990 *Proc 5th International Symposium on Polarization and Correlation in Electronic and Atomic Collisions (Hoboken)* (NIST Special Publication no 789) ed P A Neill, K H Becker and M A Kelley (Washington, DC: US Dept of Commerce) pp 128-33

Khakoo M A and McConkey J W 1987 *J. Phys. B: At. Mol. Phys.* **20** 5541-56

King S J, Neill P A and Crowe A 1985 *J. Phys. B: At. Mol. Phys.* **18** L589-94

Macek J and Jaecks D H 1971 *Phys. Rev.* A **4** 2288-300

Machado L E, Leal E P and Csanak G 1982 *J. Phys. B: At. Mol. Phys.* **15** 1773-84

Madison D H and Winters K H 1983 *J. Phys. B: At. Mol. Phys.* **16** 4437-50

Martus K E and Becker K 1989 *J. Phys. B: At. Mol. Opt. Phys.* **22** L497-502

Martus K E, Becker K and Madison D H 1988 *Phys. Rev.* A **38** 4876-9

McConkey J W, van der Burgt P J M, Corr J J and Plessis P 1990 *Proc. 5th Int. Symp. on Polarization and Correlation in Electronic and Atomic Collisions (Hoboken)* (NIST Special Publication no 789) ed P A Neill, K H Becker and M A Kelley (Washington, DC: US Dept of Commerce) pp 115-20

Meneses G D, da Paxiao F J and Padial N T 1985 *Phys. Rev.* A **32** 156-65

Murray A J, Webb C J, MacGillivray W R and Standage M C 1989 *Phys. Rev. Lett.* **62** 411-4

Nienhuis G 1979 *Theorie van Polarisatie-Effecten van Atomen en Moleculen*, unpublished lecture notes (The Netherlands: University of Utrecht)

Nienhuis G 1980 *Coherence and Correlation in Atomic Physics* ed H Kleinpoppen and J F Williams (New York: Plenum) pp 121-32

Nishimura H, Danjo A and Takahashi A 1986 *J. Phys. B: At. Mol. Phys.* **19** L167-72

Olander D R and Kruger V 1970 *J. Appl. Phys.* **41** 2769-76

O'Neill E L 1963 *Introduction to Statistical Optics* (Reading, MA: Addison Wesley)

Plessis P, Khakoo M A, Hammond P and McConkey J W 1988 *J. Phys. B: At. Mol. Opt. Phys.* **21** L483-8

Register D F, Trajmar S, Csanak G, Jensen S W, Fineman M A and Poe R T 1983 *Phys. Rev.* A **28** 151–60
Simon T, Sohn M, Hanne G F and Bartschat K 1990 *J. Phys. B: At. Mol. Opt. Phys.* **23** L259–63
Slevin J A and Chwirot S 1990 *J. Phys. B: At. Mol. Opt. Phys.* **23** 165–210
Westerveld W B, Becker K, Zetner P W, Corr J J and McConkey J W 1985 *Appl. Opt.* **24** 2256–62
Wolcke A, Bartschat K, Blum K, Borgmann H, Hanne G F and Kessler J 1983 *J. Phys. B: At. Mol. Phys.* **16** 639–55
Zetner P W, Trajmar S, Csanak G and Clark R E H 1989 *Phys. Rev.* A **39** 6022–5
Zetner P W, Trajmar S and Csanak G 1990 *Phys. Rev.* A **41** 5980–99